Physics Letters A 384 (2020) 126441

Contents lists available at ScienceDirect

Physics Letters A

www.elsevier.com/locate/pla

Solitary waves in the resonant nonlinear Schrödinger equation: Stability and dynamical properties

F. Williams [a], F. Tsitoura [a,*], T.P. Horikis [b], P.G. Kevrekidis [a,c]

[a] Department of Mathematics and Statistics, University of Massachusetts Amherst, Amherst, MA 01003-4515, USA
[b] Department of Mathematics, University of Ioannina, Ioannina 45110, Greece
[c] Mathematical Institute, University of Oxford, Oxford, UK

ARTICLE INFO

Article history:
Received 3 March 2020
Received in revised form 24 March 2020
Accepted 27 March 2020
Available online 30 March 2020
Communicated by B. Malomed

Keywords:
Resonant NLS equation
Bright and dark solitons
Stability

ABSTRACT

The stability and dynamical properties of the so-called resonant nonlinear Schrödinger (RNLS) equation, are considered. The RNLS is a variant of the nonlinear Schrödinger (NLS) equation with the addition of a perturbation used to describe wave propagation in cold collisionless plasmas. We first examine the modulational stability of plane waves in the RNLS model, identifying the modifications of the associated conditions from the NLS case. We then move to the study of solitary waves with vanishing and nonzero boundary conditions. Interestingly the RNLS, much like the usual NLS, exhibits both dark and bright soliton solutions depending on the relative signs of dispersion and nonlinearity. The corresponding existence, stability and dynamics of these solutions are studied systematically in this work.

1. Introduction

Physical phenomena involving the ingredients of dispersion and nonlinearity are usually described by nonlinear partial differential equations termed evolution equations [1]. A particularly interesting category of these are the so-called integrable systems which, besides their physical significance, also exhibit remarkable mathematical properties [2]. Key to the study of these equations is, as one might expect, their wave solutions. The Inverse Scattering Transform (IST) was developed to provide the mechanism to systematically address such systems [2]. When the IST methodology is applicable, remarkable properties can be found, such as an infinity of conserved quantities, analytical single- and multi-soliton solutions etc. Two equations stand out because they are both physically important (in fact often thought of as *universal*, due to their wide range of applications) and they initiated the field of integrable systems: the Korteweg-de Vries (KdV) and nonlinear Schrödinger (NLS) models. The former is a prototypical model for shallow water waves while the latter is most commonly used to describe quasi-monochromatic light propagation in optical media [1].

However, even these universal systems need to be amended in order for different phenomena to be incorporated when considering specific mechanisms [3]. In this case, non-integrable perturbations naturally emerge in these broadly applicable models, such as the NLS equation which has been relevant to optical, atomic and water wave systems among others [4,5]. Here, we focus on a variant of the NLS equation which is often used to describe the transmission of uni-axial waves in a cold collisionless plasma subject to a transverse magnetic field [6–8]. This system has quite similar features to the regular NLS equation, most notably exhibiting bright and dark solitons depending on the relative sign of a specific parameter (discussed below).

In its general form the resonant nonlinear Schrödinger (RNLS) equation [6–8] reads:

$$i\partial_t\Psi + \partial_x^2\Psi + \gamma(-1)^{n+1}|\Psi|^{2n}\Psi = \delta\frac{\partial_x^2|\Psi|}{|\Psi|}\Psi, \tag{1}$$

where $\Psi(x,t)$ is the complex wave profile, x, t are the spatial and temporal variables respectively and $\gamma, \delta \in \mathbb{R}$ correspond to the coefficients of the nonlinear terms. The last term of the equation involving $|\Psi|_{xx}/|\Psi|$, where the subscript stands for differentiation with respect to x, represents the de Broglie quantum potential, and can also be viewed as a diffraction term [9]. Its coefficient, namely δ, plays a crucial role in the form of the general RNLS equation (1), as it describes solutions with different behavior, depending on the regions that are separated from the critical value $\delta = 1$ [8]. More specifically, for $\delta < 1$, Eq. (1) bears connections to the NLS equation with a power law nonlinearity. For $n = 1$, it admits bright and dark soliton solutions, for $\gamma > 0$ and $\gamma < 0$ respectively. On the other hand, for $\delta > 1$ Eq. (1) has been shown to reduce to a reaction-diffusion system (RDS) which in turn represents the simplest two-component integrable system contained in the AKNS

* Corresponding author.
E-mail address: ftsitoura@gmail.com (F. Tsitoura).

https://doi.org/10.1016/j.physleta.2020.126441
0375-9601/

hierarchy of integrable systems [8,10]. It is worth noting that similar to the RNLS models involving nonlinear modifications of the dispersion term are of continued interest also in other fields such as nonlinear optics; see, e.g., [11] for a recent (albeit somewhat different in flavor) example.

The exact solutions of Eq. (1) have long been discussed in the literature and with many different methods (including the first integral method, the G'/G expansion, the Darboux-Bäcklund transformation and the Hirota bilinear method, among others) [12–19]. Here, and for completeness we will also derive the solitary waves of the equation but will focus mainly on their stability properties. Below, we also discuss briefly, for completeness, some of the important properties of the equation and refer the interested reader to Refs. [6–8] for more details.

2. Properties

The Madelung transformation decomposes the wavefunction as $\Psi = e^{R-iS}$ where $R = R(x,t)$ and $S = S(x,t)$ are real-valued functions. It follows directly that Eq. (1) is equivalent to the system of equations

$$\begin{aligned} &\partial_t R - \partial_x^2 S - 2\partial_x R \partial_x S = 0, \\ &\partial_t S + (1-\delta)\left(\partial_x^2 R + (\partial_x R)^2\right) - (\partial_x S)^2 + \gamma(-1)^{n+1} e^{2nR} = 0. \end{aligned} \tag{2}$$

First, we consider the case with $\delta < 1$ and rescale time and phase of the wave function according to $t = (1-\delta)^{\frac{1}{2}}\tilde{t}$ and $S = (1-\delta)^{\frac{1}{2}}\tilde{S}(x,\tilde{t})$, respectively. By applying the above transformations to Eq. (2), we get the new system for the phase and amplitude

$$\begin{aligned} &\partial_{\tilde{t}} R - \partial_x^2 \tilde{S} - 2\partial_x R \partial_x \tilde{S} = 0, \\ &\partial_{\tilde{t}} \tilde{S} + \partial_x^2 R + (\partial_x R)^2 - \left(\partial_x \tilde{S}\right)^2 + \frac{\gamma}{1-\delta} e^{2nR} = 0, \end{aligned} \tag{3}$$

which, for the new complex wave function $\tilde{\Psi} = e^{R-i\tilde{S}}$, corresponds to the NLS equation:

$$i\partial_{\tilde{t}}\tilde{\Psi} + \partial_x^2\tilde{\Psi} + \frac{\gamma}{1-\delta}|\tilde{\Psi}|^{2n}\tilde{\Psi} = 0. \tag{4}$$

For $n = 1$, the NLS equation, Eq. (4), for $\gamma < 0$ is of the defocusing type and describes black soliton solutions in BECs, nonlinear optics, water waves and in many other systems. For $\gamma > 0$, it admits bright soliton solutions.

However, when $\delta > 1$, the landscape of solutions of Eq. (1) differs. To illustrate this, we introduce the transformations $t = (\delta-1)^{\frac{1}{2}}\tilde{t}$ and $S = (\delta-1)^{\frac{1}{2}}\tilde{S}(x,\tilde{t})$ and apply them to Eq. (2). In particular, upon setting

$$r = \exp\left(R(x,\tilde{t}) + \tilde{S}(x,\tilde{t})\right), \tag{5}$$

$$s = -\exp\left(R(x,\tilde{t}) - \tilde{S}(x,\tilde{t})\right), \tag{6}$$

and by dropping the tildes, we obtain the following reaction-diffusion (RDS) system

$$r_t - r_{xx} + Br^{n+1}s^n = 0, \tag{7}$$

$$s_t + s_{xx} - Br^n s^{n+1} = 0, \tag{8}$$

where $B = -\gamma/(\delta-1)$. It is particularly intriguing that from a conservative (indeed, Hamiltonian, as is discussed below) system, we have obtained a system featuring reaction and diffusion in one of the components, along with reaction and *anti-diffusion* in the second one. Yet, we note that this system bears gain and loss (notice the opposite signs in the nonlinear terms in Eqs. (7)-(8)) and can thus be brought under the umbrella of so-called $\mathcal{PT}$-symmetric systems [20], as shown next. A number of few degree-of-freedom systems of that form [21] (i.e., ones that could be mapped from Hamiltonian to $\mathcal{PT}$ symmetric or vice-versa) has already been reported, whereas very recently $\mathcal{PT}$-symmetric systems at the level of partial differential equations [22] have also been proposed and studied including the $\mathcal{PT}$-symmetric extensions of the massive Thirring and the Gross-Neveu models.

2.1. Space-time invariance and Galilean symmetry of the RDS

For the general case where n is arbitrary, we investigate the time and space invariance of the system (7)-(8). We find that the system is invariant under the $\mathcal{PT}$ transformation, where the operators $\mathcal{P}$ and $\mathcal{T}$ acting on the real valued functions $r(x,t)$ and $s(x,t)$ are given by

$$\mathcal{P}\begin{pmatrix} r(x,t) \\ s(x,t) \end{pmatrix} = \begin{pmatrix} s(x,t) \\ r(x,t) \end{pmatrix}, \tag{9}$$

for the parity operator $\mathcal{P}$, while the time-reversal operator $\mathcal{T}$ is defined as:

$$\mathcal{T}\begin{pmatrix} r(x,t) \\ s(x,t) \end{pmatrix} = \begin{pmatrix} r(x,-t) \\ s(x,-t) \end{pmatrix}. \tag{10}$$

Consequently the $\mathcal{PT}$ operator acting on the functions r and s is as follows:

$$\mathcal{PT}\begin{pmatrix} r(x,t) \\ s(x,t) \end{pmatrix} = \begin{pmatrix} s(x,-t) \\ r(x,-t) \end{pmatrix}. \tag{11}$$

The action of the $\mathcal{PT}$ operator on the system (7)-(8), and the resulting invariance reveals the parity-time symmetry of the model. Next, we investigate whether the RDS has Galilean symmetry invariance. For a fixed velocity parameter, namely υ, we define $a(x,t) = \frac{\upsilon}{2}x + \frac{\upsilon^2}{4}t$ and the usual Galilean transformation $x' = x - \upsilon t$ as well as $t' = t$ can be considered. By plugging

$$\tilde{r}(x,t) = e^{-a(x',t')} r(x',t') = e^{-\frac{\upsilon}{2}x + \frac{\upsilon^2}{4}t} r(x-\upsilon t, t), \tag{12}$$

$$\tilde{s}(x,t) = e^{a(x',t')} s(x',t') = e^{\frac{\upsilon}{2}x - \frac{\upsilon^2}{4}t} s(x-\upsilon t, t), \tag{13}$$

to the system (7)-(8) we obtain

$$\tilde{r}_t - \tilde{r}_{xx} + B\tilde{r}^{n+1}\tilde{s}^n = 0, \tag{14}$$

$$\tilde{s}_t + \tilde{s}_{xx} - B\tilde{r}^n\tilde{s}^{n+1} = 0, \tag{15}$$

which highlights the Galilean invariance of the RDS. Equivalently, a more general solution $\tilde{\Psi}$ can be constructed by applying the Galilean transform to Ψ. To do so, if $\Psi = e^{R-iS}$ is a solution of (1), so is $\tilde{\Psi}$ where

$$\tilde{\Psi}(x,t) = e^{i\left[\frac{\upsilon}{2}x - \frac{\upsilon^2}{4}t\right]}\Psi(x-\upsilon t, t), \tag{16}$$

for any real number υ, (R, S are real-valued again). The above follows from the equivalence of the solutions of (1) with solutions of the corresponding Madelung fluid equations, which in turn are equivalent with solutions of a corresponding general RDS which was already proven to be Galilean invariant.

2.2. Integrals of motion and Lagrangian formulation

Eq. (1) has also been studied with integrable systems tools (the so-called direct methods) like the Hirota [7] and Bäcklund-Darboux

[8] transformations. The first three conserved quantities, for $n=1$, are found to be:

$$N=\int_{-\infty}^{\infty}|\Psi|^2dx, \tag{17}$$

$$P=i\int_{-\infty}^{\infty}\left(\Psi_x^*\Psi-\Psi_x\Psi^*\right)dx, \tag{18}$$

$$E=\int_{-\infty}^{\infty}\left(\Psi_x^*\Psi_x-\delta\left(|\Psi|_x\right)^2-\frac{\gamma}{2}|\Psi|^4\right)dx. \tag{19}$$

In different contexts these integrals represent different physical quantities. For example, the first may correspond to the number of atoms in Bose-Einstein condensates or to the energy of a pulse in optics. The Lagrangian of the RNLS (1) (again for $n=1$) reads

$$\mathcal{L}_{\Psi,\Psi^*}=\frac{i}{2}\left(\Psi^*\Psi_t-\Psi_t^*\Psi\right)-\Psi_x^*\Psi_x+\delta\left(|\Psi|_x\right)^2+\frac{\gamma}{2}|\Psi|^4, \tag{20}$$

hence the RNLS is obtained from the Euler-Lagrange equations thereof.

Since $\Psi(x,t)=\mathrm{e}^{R-iS}$, the Lagrangian (20) can also be rewritten

$$\mathcal{L}_{R,S}=\mathrm{e}^{2R}\left[S_t-S_x^2+(\delta-1)R_x^2\right]+\frac{\gamma}{2}\mathrm{e}^{4R}. \tag{21}$$

We conclude our discussion in this Section by expressing R,S in terms of r,s. Let

$$\begin{aligned}R(x,t)&=\tilde{R}(x,\beta t)=\frac{1}{2}\left[\log r(x,\beta t)+\log\left(-s(x,\beta t)\right)\right],\\ S(x,t)&=\beta\tilde{S}(x,\beta t)=\frac{\beta}{2}\left[\log r(x,\beta t)-\log\left(-s(x,\beta t)\right)\right],\end{aligned} \tag{22}$$

where $\beta=\sqrt{\delta-1}$. Then, the Lagrangian becomes

$$\mathcal{L}_{r,s}=sr_t-rs_t+2r_xs_x+Br^2s^2 \tag{23}$$

with the Euler-Lagrange equations coinciding with the system of Eqs. (7)-(8).

3. Stability analysis

A natural next step is to examine the stability of some of the simplest solutions of the RNLS model in the form of plane wave solutions $\Psi(x,t)=A_0\exp[i(kx-\omega t)]$, with A_0, k and ω being the amplitude, wavenumber and frequency, respectively, of Eq. (1), with $n=1$, by performing the standard modulation instability (MI) analysis. To that effect, we consider the stability for the most trivial case where $k=0$ and $A_0=\sqrt{-\omega/\gamma}$. In that realm, we introduce the following ansatz

$$\begin{aligned}\Psi(x,t)&=(\Psi_0+\epsilon b(x,t))\exp[i(-\omega t+\epsilon w(x,t))],\\ &0<\epsilon\ll 1,\end{aligned} \tag{24}$$

and plug it into Eq. (1). The amplitude and phase perturbations assume the form $b(x,t)=b_0\exp(i(Qx-\Omega t))$ and $w(x,t)=w_0\exp(i(Qx-\Omega t))$ where b_0 and w_0 are constants whereas Q and Ω are the perturbation wavenumber and frequency, respectively. At order $\mathcal{O}(\epsilon)$, the following dispersion relation is obtained

$$\Omega^2=Q^2\left[(1-\delta)Q^2-2\gamma A_0^2\right], \tag{25}$$

that links the perturbation wavenumber, frequency and amplitude of the solution. When $\delta=0$, Eq. (25) coincides with the respective dispersion relation of the NLS equation [4,5]. In particular, the results arising from the stability analysis of the NLS equation and for $\gamma=-1$ suggest the absence of that instability and the plane waves are spectrally stable. On the other hand, for the focusing NLS case with $\gamma=1$, we expect that small perturbations with wavenumbers $Q<Q_{cr}=A_0\sqrt{2\gamma}$, on top of the plane wave solution, will grow over time. For the RNLS equation with $\delta<1$, the MI analysis results are similar to the ones of the NLS equation. More specifically, and for $\gamma<0$, there is no modulation instability, and thus the plane waves persist. As such, localized solutions of interest may occur on top of a plane wave background, whereas for $\gamma>0$, we expect that suitable small perturbations will grow over time for $Q<Q_{cr}=A_0\sqrt{2\gamma/(1-\delta)}$ in that case. On the other hand, when $\delta>1$, and for any value of γ, small perturbations with wavenumbers $Q^2>2A_0^2\gamma/(1-\delta)$ grow over time. Thus, we expect instabilities to occur in the focusing case of $\gamma>0$; additionally, an unstable regime emerges even for the defocusing case of $\gamma<0$, but for small-wavelength perturbations contrary to the $\gamma<0$, $\delta<1$ setting. The above analysis, suggests two different regimes in the parameter δ, that is, $\delta<1$ and $\delta>1$. We will treat the cases with $\delta<1$ and $\gamma<0$, and $\delta>1$ (for all values of γ), called scenarios A and B hereafter.

It is therefore relevant to show the dynamical evolution of plane wave solutions in those two cases. The results confirming the MI analysis are depicted in Fig. 1 for both scenarios A (left panels) and B (right panels), respectively. In particular, these panels correspond to densities $|\Psi(x,t)|^2$ for the initial condition $\Psi(x,t=0)=1$ perturbed by a sine function of amplitude of $\mathcal{O}\left(10^{-3}\right)$ that has a wavenumber Q of $Q=2$. When $\delta<1$ and $\gamma=-1$ (left panels), there are no signs of instability, as predicted from Eq. (25); indeed, the initial small perturbations remain small for the remainder of the evolution. However when $\delta>1$ (right panels) the plane wave solution is highly unstable. The initial small perturbation of the plane wave exhibits exponential growth almost immediately resulting in the rapid deviation from the homogeneous background solution. Note, here the different time scales on the left ($0<t<1000$) and the right ($0<t<0.004$). It should be noted that we numerically integrate Eq. (1) in time using a finite difference scheme for the spatial discretization and the Runge-Kutta method for the time marching. The resolution of the spatial discretization is $dx=0.02$ and the time step-size is $dt=10^{-4}$ for the left panels and $dt=10^{-6}$ for the right panels of Fig. 1.

3.1. Linear stability analysis of the stationary states

Once a steady state solution is available, we can explore their potential robustness. Towards this direction, we use the linear stability analysis, and upon linearizing Eq. (1) around a steady state, we find its excitation spectrum. The scope of this analysis is to identify the fate of small perturbations on top of an already known solution. If $\phi(x)$ stands for a steady state, we consider small perturbations through the ansatz:

$$\Psi(x,t)=\mathrm{e}^{-i\mu t}\left\{\phi(x)+\epsilon\left[u(x)\,\mathrm{e}^{-i\omega t}+v^*(x)\,\mathrm{e}^{i\omega^* t}\right]\right\}, \tag{26}$$

where ω is the (potentially) complex eigenfrequency, i.e. $\omega=\omega_r+i\omega_i$ and (u,v) are the perturbation eigenmodes. After plugging the ansatz (26) into Eq. (1) and keeping terms of order $\mathcal{O}(\epsilon)$, we derive the eigenvalue problem:

$$\begin{bmatrix}L_1 & L_2\\ -L_2^* & -L_1^*\end{bmatrix}\begin{bmatrix}u\\ v\end{bmatrix}=\omega\begin{bmatrix}u\\ v\end{bmatrix}, \tag{27}$$

where L_1 and L_2 are given by

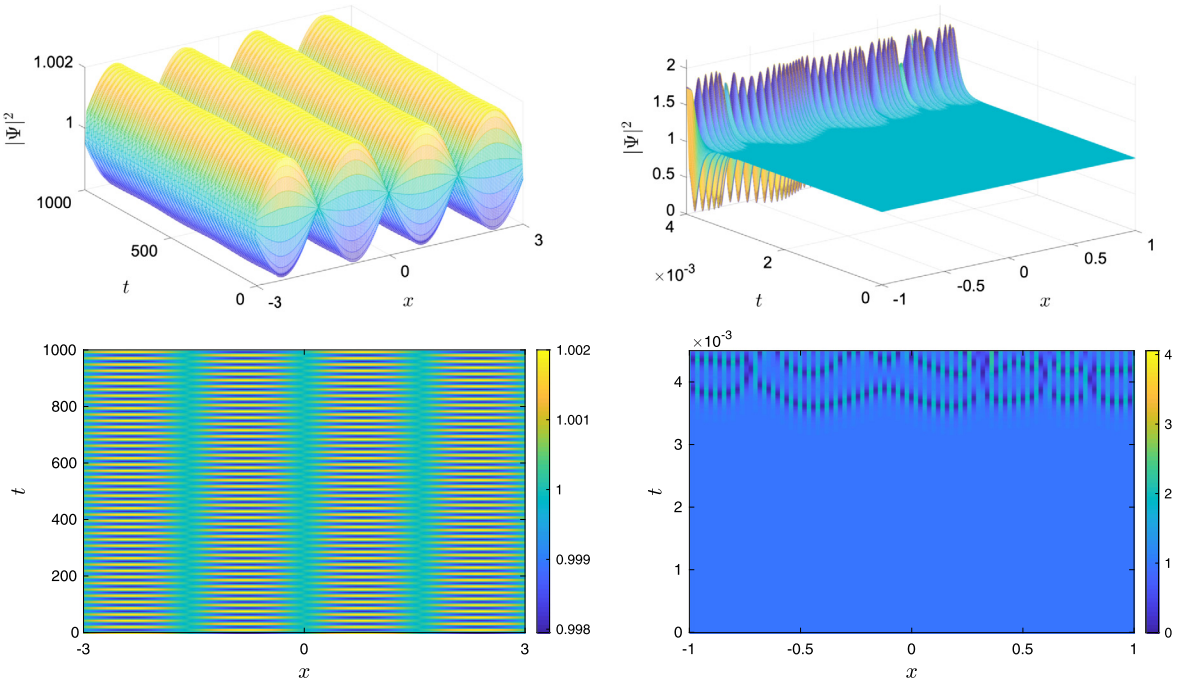

Fig. 1. Mesh (upper panels) and contour (bottom panels) plots of plane wave evolution of the RNLS equation for $\delta < 1$ and $\delta > 1$ shown in the left and right panels respectively. The initial condition is $\Psi(x, t = 0) = 1$ perturbed by a sine function (see text for details). The parameters used are $\delta = 0.99$ and $\gamma = -1$, and $\delta = 2$, $\gamma = -1$, in the left and right panels respectively.

$$L_1 = -\left(1 - \frac{\delta}{2}\right)\partial_{xx} + \frac{\delta}{4}\left(-2\left(\frac{\phi_x}{\phi} - \frac{\phi_x^*}{\phi^*}\right)\partial_x + \left(\frac{\phi_x}{\phi}\right)^2 - \left(\frac{\phi_x^*}{\phi^*}\right)^2 + 2\frac{\phi_{xx}^*}{\phi^*}\right) - \mu - \gamma\,(-1)^{n+1}\,(n+1)\,|\phi|^{2n}, \tag{28}$$

$$L_2 = \frac{\delta}{2}\left(\frac{\phi}{\phi^*}\partial_{xx} + \left(\frac{\phi_x}{\phi^*} - \frac{\phi\phi_x^*}{(\phi^*)^2}\right)\partial_x - \frac{|\phi_x|^2}{(\phi^*)^2} + \frac{\phi\left(\phi_x^*\right)^2}{(\phi^*)^3} - \frac{\phi\phi_{xx}^*}{(\phi^*)^2}\right) - \gamma\,(-1)^{n+1}\,n\phi^2|\phi|^{2(n-1)}. \tag{29}$$

For the simplest case where $n = 1$ and $\phi(x) \in \mathbb{R}$, the above matrix elements assume the much simpler form

$$L_1 = -\left(1 - \frac{\delta}{2}\right)\partial_{xx} + \frac{\delta}{2}\frac{\phi_{xx}}{\phi} - 2\gamma\phi^2 - \mu, \tag{30}$$

$$L_2 = \frac{\delta}{2}\left(\partial_{xx} - \frac{\phi_{xx}}{\phi}\right) - \gamma\phi^2. \tag{31}$$

Steady states are numerically identified by using the Newton-Raphson method, although as we will see below they are often available in closed analytical form for the steady states waveforms of the present model. Then their spectrum (ω_r, ω_i) is obtained by solving numerically the eigenvalue problem of Eq. (27). When the spectrum has purely real eigenfrequencies, then the corresponding steady state is dynamically *stable*. The presence of complex eigenfrequencies in the spectrum indicates that the particular steady state is unstable, i.e., that small perturbations lead either to an exponential growth (for purely imaginary eigenfrequencies) or to an oscillatory instability of the solution (for genuinely complex ones – although such a scenario will not be encountered in what follows). In the sections that follow, we are going to investigate the solutions that exist for scenarios *A* and *B* and monitor their stability and associated dynamics.

4. Scenario A: soliton solutions for $\delta < 1$ and $\gamma < 0$

This case scenario corresponds to $\gamma < 0$ and $\delta < 1$. A fundamental solution that can be obtained in this effectively (still) defocusing case is the dark soliton solution, and its existence, stability and dynamics will be investigated in what follows.

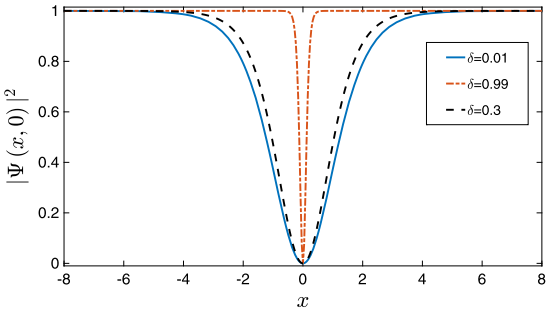

Fig. 2. Densities of the stationary dark solitons for three different values of the parameter δ of $\delta = 0.01$ (solid blue), $\delta = 0.3$ (dashed black line), and $\delta = 0.99$ (dashed-dotted red line), respectively. The other parameter values are: $\gamma = -1$ and $\mu = -1$. (For interpretation of the colors in the figure(s), the reader is referred to the web version of this article.)

4.1. Exact solutions

For the case of cubic nonlinearity ($n = 1$), Eq. (1) possesses dark soliton solutions of the form

$$\Psi(x, t) = \sqrt{-\mu}\tanh\left(\sqrt{\frac{-\mu}{2(1-\delta)}}x\right)e^{i\mu t}, \quad \mu < 0, \tag{32}$$

where we set $\mu = -1$ in the analysis that follows. Solution (32) could be directly obtained from the Duffing equation

$$-\tilde{u}_{xx} + 2\tilde{u}^3 + \tilde{\mu}\tilde{u} = 0$$

with $\tilde{u} = \sqrt{\tilde{\gamma}/2}u$, $\tilde{\mu} = \mu/(1-\delta)$ and $\tilde{\gamma} = \tilde{\mu}/\mu$, which originates from (1) after employing the ansatz $\Psi(x, t) = e^{i\mu t}u$. For $\delta = 0$, Eq. (32) gives the well-known dark soliton solution of the defocusing NLS equation. Fig. 2 illustrates solution profiles for three different values of δ of $\delta = 0.01, 0.3$ and 0.99 (see the legend therein). We

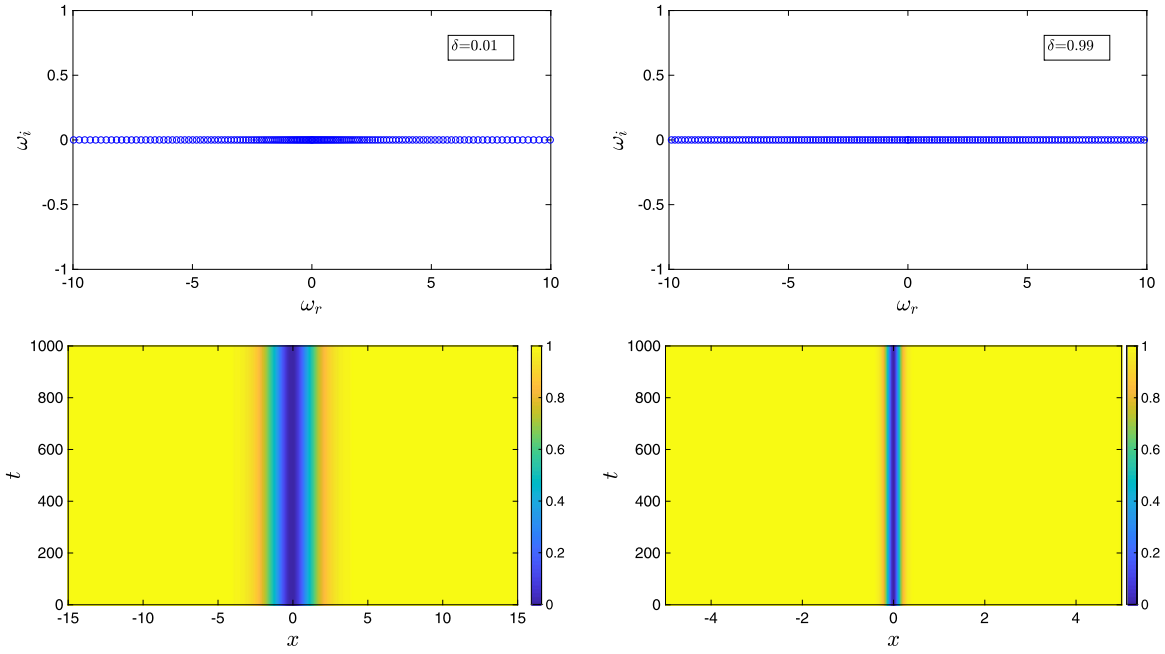

Fig. 3. *Top panels*: The corresponding spectral planes for the cases $\delta = 0.01$ and 0.99 are shown in the left and right panels respectively. *Bottom panels*: Contour plots showing the dynamical evolution of the dark soliton solutions confirming their predicted dynamical stability. The left panel shows the case with $\delta = 0.01$ and the right panel the case with $\delta = 0.99$. The other parameter values used are $\gamma = -1$ and $\mu = -1$.

observe that as we go towards the upper limit in δ, the width of the solution is decreasing.

4.2. Numerical results

Upon numerically identifying the above exact solutions using the Newton-Raphson method, we proceed to solve the eigenvalue problem (27) numerically. The corresponding spectra of the solution (32) are presented in the top panels of Fig. 3 for the cases with $\delta = 0.01$ (top left panel) and $\delta = 0.99$ (top right panel), respectively, i.e., the two limits: the NLS and the infinitesimal width case. We studied systematically the spectra for all the values of δ in the range $\delta \in (0, 1)$ and found that all the eigenfrequencies are lying on the real axis, thus suggesting that the solutions are spectrally stable for all δ in this interval. It is natural to explore the robustness of solutions (32) by integrating Eq. (1) forward in time. To that end, we have used finite differences for the spatial discretization with $dx = 0.02$ and the Runge-Kutta method for the time evolution with $dt = 10^{-4}$. The results from the simulations are shown in the bottom left and right panels of Fig. 3 for the cases with $\delta = 0.01$ and $\delta = 0.99$, respectively. In both cases, the solitons remain robust for the time intervals considered therein.

5. Scenario B: soliton solutions for $\delta > 1$

5.1. Theoretical background and exact solutions of the general RNLS equation

We construct a traveling wave solution of the generalized RNLS (1) by assuming $\Psi(x,t) = \phi(x - \upsilon t)\, e^{i(-\kappa x + \omega t + \theta)}$, where $\phi(w) > 0$, $w = x - \upsilon t$, and $\kappa, \omega, \theta, \upsilon \in \mathbb{R}$.

In the present case $R(x,t) = \log \phi(x - \upsilon t)$ and $S(x,t) = \kappa x - \omega t - \theta$. Then by substituting these transformations into Eqs. (2) with the assumption that $\phi(w)$ is not a constant function, we obtain the conditions:

$$\phi''(w) + a\phi(w) = \lambda \phi(w)^{2n+1}, \qquad a = \frac{(\omega + \kappa^2)}{\delta - 1}, \quad \lambda = -\gamma \frac{(-1)^n}{\delta - 1}. \tag{33}$$

The traveling wave solution can then be found in the form $\phi(w) = A[\mathrm{sech}(\alpha w)]^{1/n}$ with suitably constants $A > 0$ and α [4]. The resulting waveform and associated algebraic conditions for A, ω, κ and υ read:

$$\Psi(x,t) = A\big[\mathrm{sech}\left(\alpha\left(x - \upsilon t\right)\right)\big]^{\frac{1}{n}} e^{i(-\kappa x + \omega t + \theta)}, \tag{34}$$

with

$$\omega = -(\delta - 1)\frac{\alpha^2}{n^2} - \kappa^2, \quad \kappa = -\frac{\upsilon}{2}, \qquad A = \left[\frac{-\left(\omega + \kappa^2\right)(n+1)}{\gamma(-1)^n}\right]^{\frac{1}{2n}}, \quad \gamma(-1)^n > 0, \tag{35}$$

where θ is an arbitrary phase. Also, we should note that the last condition implies that n should be odd for $\gamma < 0$, whereas n should be even for $\gamma > 0$.

5.2. Numerical results

We examine the relevant theoretical prediction in the prototypical case of $n = 1$ for stationary solutions with $\upsilon = 0$. In that case, the associated bright solitary waveform becomes:

$$\Psi_0(x) = \alpha \sqrt{\frac{2(1-\delta)}{\gamma}}\, \mathrm{sech}(\alpha x). \tag{36}$$

We again identify numerically the steady states of Eq. (36) by using the Newton-Raphson method. As initial guess we use the exact solution Ψ_0 (which naturally constitutes an excellent initial guess, as it is exact up to the local truncation error). We have investigated two different sets of parameters; the first corresponds to $\delta = 1.01$, $\gamma = -1$ and $\alpha = 0.8$, and the second to $\delta = 2$, $\gamma = -1$ and $\alpha = 0.8$. The respective profiles of the exact solutions Ψ_0 (red circles) and the numerically exact solutions Ψ (blue line) are shown in the top left and right panels of Fig. 4. The bottom panels of the same figure show the associated spectral planes. It can be appreciated that the modes are extremely unstable in this case. This is rather natural to expect as the point spectrum of the solitary wave consists

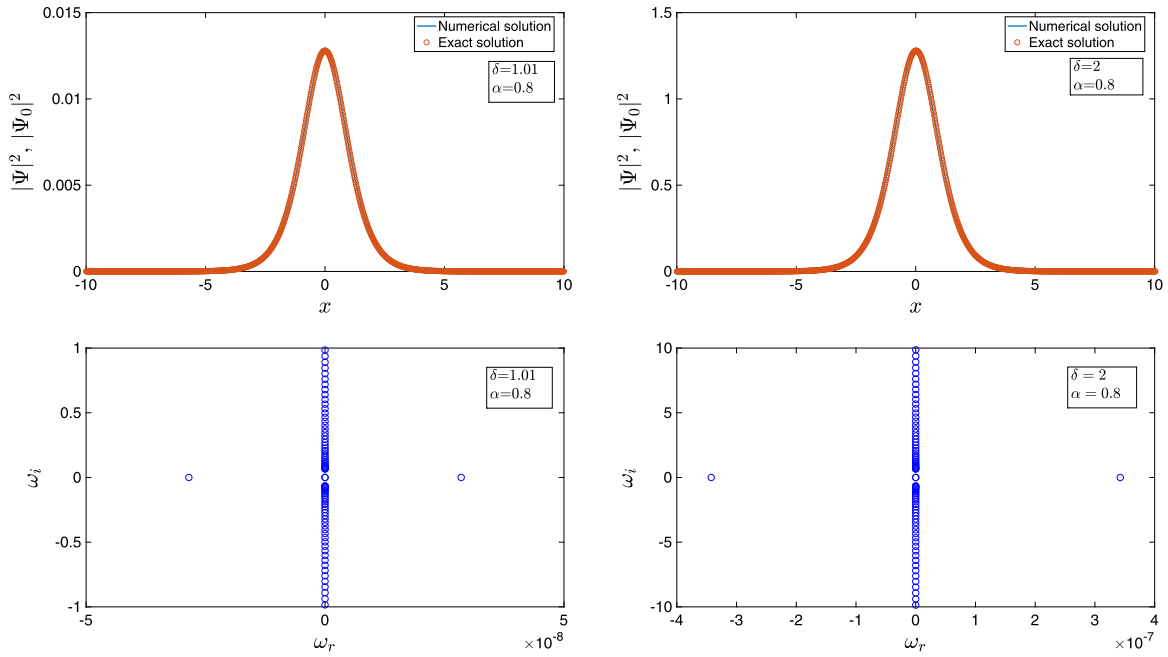

Fig. 4. *Top panels*: Densities of the exact (red circles) and the numerical (solid blue) steady state solutions of Eq. (36) for $\delta = 1.01$ (left panel) and $\delta = 2$ (right panel). *Bottom panels*: The corresponding spectral planes. The other parameter values used are $n = 1$, $\upsilon = 0$, $\gamma = -1$, $\alpha = 0.8$ and $\omega = -1$.

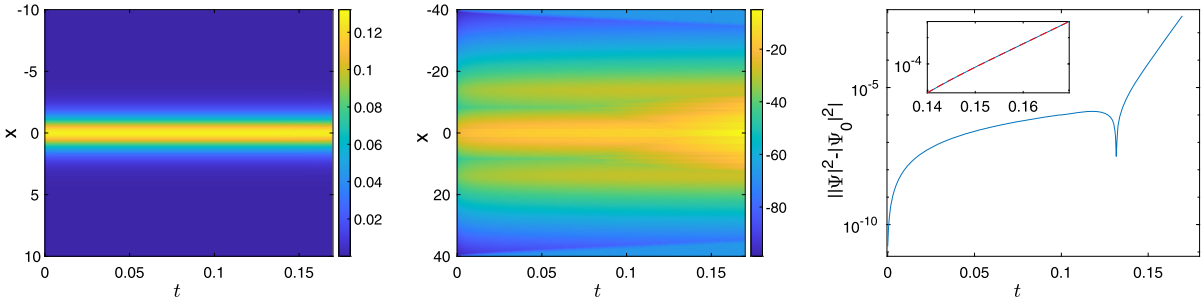

Fig. 5. An example of the case with $\gamma = -1$ and $\delta = 1.1$ is given. The left panel shows the space-time evolution of the norm, where the instability is essentially indiscernible over the time scale $[0, 0.17]$ shown. The middle panel shows the (logarithm of the absolute value of the) difference of the solution intensity from the initial condition (Ψ_0) intensity in its space-time evolution. Here the dramatic growth of the error is evident (not only weakly on the boundaries but also more clearly) in the center of the domain. Finally, in the right panel what is shown is the quantity of the middle panel specifically at $x = 0$ as a function of time. This density difference is shown at $x = 0$ as a function of time t in a semilog plot. The inset shows the exponential part of the growth with the best fit over more than two orders of magnitude. The best fit slope (i.e., the instability growth rate) is 208.6.

solely of the $\omega = 0$ eigenfrequency pairs due to the translational and phase symmetries. However, the continuous spectrum of the problem lies entirely on the imaginary axis reflecting the modulational instability of the background, as per Eq. (25). We note in passing that rather similar results were found for the case of $\gamma < 0$ and odd n, as well as for that of $\gamma > 0$ and even n.

Here it is important to discuss the dynamical evolution of the bright soliton solutions for the cases with $\delta > 1$ that were studied above. Notice that the stability analysis indicates that the solution is wildly unstable with growth rates (of the background equilibrium state) extending over an interval up to $\omega_i = Q^2\sqrt{\delta - 1}$. The maximal Q corresponds to the minimal length scale dx of the domain, according to $Q = 2\pi/dx$ and is typically of the order of many hundreds. Thus, it should come as no surprise in Fig. 5 that even when starting with the exact analytical bright solitary wave solution with no perturbation (other than round off error), eventually the relevant instability takes over and grows with a rate that in the present example is found to be approximately 208.6. In the figure, the maximal density evolution is shown by comparing to the density of the (exact solution) initial condition, along with the left panel of the space-time profile of the solution. The latter shows no discernible signs of instability over the time scale shown. The middle panel shows the space-time evolution of the difference $\log(||\Psi|^2 - |\Psi_0|^2|)$. The extremely rapid exponential nature of the growth (with this extremely high growth rate) is rather transparent within the middle and right panels of the figure, in line with our theoretical prediction about the highly unstable nature of the $\delta > 1$ dynamics.

6. Conclusions

We have investigated a more general form of the RNLS equation with power-law nonlinearity. This equation, similar to the RNLS with a cubic nonlinearity, behaves differently for different values of the coefficient of the de Broglie potential, relevant to the cold collisionless plasma system of interest here. More specifically, for $\delta < 1$, it reduces to the standard NLS equation with a power law nonlinearity via a suitable transformation. We investigated dark solitons for different values of the parameter δ and we observed that they are dynamically stable solutions as our linear stability analysis suggests and numerical simulations corroborate. On the other hand, when $\delta > 1$, the general RNLS reduces into a system featuring reaction and diffusion in one component while the second one has reaction and anti-diffusion. This, in turn, represents

a partial differential equation example of Hamiltonian form that can be transformed into a $\mathcal{PT}$ symmetric one. We performed a stability analysis of bright soliton solutions of the RNLS not only with $n = 1$ but also for $n > 1$ in the case of $\delta > 1$. The analysis of these states however indicated that they are all unstable at the linearized level, a feature in line with the modulational instability analysis also performed herein. This instability was shown to be associated with large growth rates evidenced in our direct numerical simulations.

Numerous further directions may be worthwhile to further pursue in this setting. Most notably deriving and examining the relevant model in higher dimensions. In its one dimensional installment and for the associated real solutions, the principal solutions of the model appear to be similar to the usual NLS ones with suitable renormalization of the dispersion coefficient. However, in higher dimension the genuinely complex nature of the associated wavefunction is more likely to make it relevant for this to no longer be the case, when considering solutions of a vortical form. There, the full role of the effect of the δ-induced perturbation may be quite intriguing to appreciate. Such topics are currently under consideration and will be reported in future studies.

Declaration of competing interest

The authors declare that they have no known competing financial interests or personal relationships that could have appeared to influence the work reported in this paper.

Acknowledgements

This material is based upon work supported by the US National Science Foundation under Grants No. PHY-1602994 and DMS-1809074 (PGK). PGK also acknowledges support from the Leverhulme Trust via a Visiting Fellowship and thanks the Mathematical Institute of the University of Oxford for its hospitality during part of this work.

References

[1] M.J. Ablowitz, Nonlinear Dispersive Waves: Asymptotic Analysis and Solitons, Cambridge University Press, 2011.
[2] M.J. Ablowitz, H. Segur, Solitons and the Inverse Scattering Transform, SIAM Studies in Applied Mathematics, 1981.
[3] E. Infeld, G. Rowlands, Nonlinear Waves, Solitons and Chaos, Cambridge Univesity Press, 1990.
[4] C. Sulem, P.L. Sulem, Nonlinear Schrödinger Equations: Self-Focusing Instability and Wave Collapse, Springer, 1999.
[5] P. Kevrekidis, D. Frantzeskakis, R. Carretero-González, The Defocusing Nonlinear Schrödinger Equation, SIAM, 2015.
[6] O.K. Pashaev, J.H. Lee, Resonance solitons as black holes in Madelung fluid, Mod. Phys. Lett. A 17 (2002) 1601–1619.
[7] J.-H. Lee, O.K. Pashaev, Solitons of the resonant nonlinear Schrödinger equation with nontrivial boundary conditions: Hirota bilinear method, Theor. Math. Phys. 152 (2007) 991–1003.
[8] J.-H. Lee, O.K. Pashaev, C. Rogers, W.K. Schief, The resonant nonlinear Schrödinger equation in cold plasma physics. Application of Bäcklund-Darboux transformations and superposition principles, J. Plasma Phys. 73 (2007) 257–272.
[9] A. Hasegawa, Y. Kodama, Solitons in Optical Communications, Clarendon Press, 1995.
[10] M.J. Ablowitz, D.J. Kaup, A.C. Newell, H. Segur, Nonlinear evolution equations of physical significance, Phys. Rev. Lett. 31 (1973) 125–127.
[11] C.-Y. Lin, J.-H. Chang, G. Kurizki, R.-K. Lee, Solitons supported by intensity-dependent dispersion, arxiv preprint, arXiv:2001.01631, 2020.
[12] M. Eslami, M. Mirzazadeh, B.F. Vajargah, A. Biswas, Optical solitons for the resonant nonlinear Schrödinger's equation with time-dependent coefficients by the first integral method, Optik 125 (2014) 3107–3116.
[13] M. Eslami, M. Mirzazadeh, A. Biswas, Soliton solutions of the resonant nonlinear Schrödinger's equation in optical fibers with time-dependent coefficients by simplest equation approach, J. Mod. Opt. 60 (2013) 1627–1636.
[14] A. Biswas, Soliton solutions of the perturbed resonant nonlinear Schrödinger's equation with full nonlinearity by semi-inverse variational principle, Quantum Phys. Lett. 1 (2012) 79–84.
[15] M. Mirzazadeh, M. Eslami, D. Milovic, A. Biswas, Topological solitons of resonant nonlinear Schrödinger's equation with dual power law nonlinearity by g'/g-expansion technique, Optik 125 (2014) 5480–5489.
[16] H. Triki, T. Hayat, O.M. Aldossary, A. Biswas, Bright and dark solitons for the resonant nonlinear Schrödinger's equation with time-dependent coefficients, Opt. Laser Technol. 44 (2012) 2223–2231.
[17] H. Triki, A. Yildirim, T. Hayat, O.M. Aldossary, A. Biswas, 1-soliton solution of the generalized resonant nonlinear dispersive Schrödinger's equation with time-dependent coefficients, Adv. Sci. Lett. 16 (2012) 309–312.
[18] H.M. Srivastava, H. Günerhan, B. Ghanbari, Exact traveling wave solutions for resonance nonlinear Schrödinger equation with intermodal dispersions and the Kerr law nonlinearity, Math. Methods Appl. Sci. 2019 (2019) 1–12.
[19] Q. Zhou, C. Wei, H. Zhang, J. Lu, H. Yu, P. Yao, Q. Zhu, Exact solutions to the resonant nonlinear Schrödinger equation with both spatio-temporal and intermodal dispersions, Proc. Rom. Acad. A 17 (2016) 307–313.
[20] V.V. Konotop, J. Yang, D.A. Zezyulin, Nonlinear waves in $\mathcal{PT}$-symmetric systems, Rev. Mod. Phys. 88 (2016) 035002.
[21] I.V. Barashenkov, Hamiltonian formulation of the standard $\mathcal{PT}$-symmetric nonlinear Schrödinger dimer, Phys. Rev. A 90 (2014) 045802.
[22] N.V. Alexeevaa, I.V. Barashenkov, A. Saxena, Spinor solitons and their $\mathcal{PT}$-symmetric offspring, Ann. Phys. 403 (2019) 198–223.